Geophysical Research Letters

RESEARCH LETTER
10.1029/2019GL084826

Key Points:
- In CESM1, extreme precipitation (the heaviest day each year) is quadratically related to warming in the tropics
- Extreme precipitation change is closely related to circulation strength and large-scale precipitation fraction
- CESM1 is an end member among its cohort of climate models for this behavior

Supporting Information:
- Supporting Information S1

Correspondence to:
A. G. Pendergrass,
apgrass@ucar.edu

Citation:
Pendergrass, A. G., Coleman, D. B., Deser, C., Lehner, F., Rosenbloom, N., & Simpson, I. R. (2019). Nonlinear response of extreme precipitation to warming in CESM1. *Geophysical Research Letters*, *46*, 10,551–10,560. https://doi.org/10.1029/2019GL084826

Received 1 AUG 2019
Accepted 29 AUG 2019
Accepted article online 3 SEP 2019
Published online 12 SEP 2019

Nonlinear Response of Extreme Precipitation to Warming in CESM1

A. G. Pendergrass[1], D. B. Coleman[1], C. Deser[1], F. Lehner[1], N. Rosenbloom[1], and I. R. Simpson[1]

[1]National Center for Atmospheric Research, Boulder, CO, USA

Abstract The response of extreme precipitation to warming varies widely among climate models, especially in the tropics. In some models, there have been indications that the rate of response increases with warming—that the response is not linear. We investigate the evolution of extreme precipitation, quantified by the maximum accumulated precipitation in a day each year, in CESM1. We find that tropical- and global-average extreme precipitation is related to global-mean surface temperature quadratically. This behavior is associated with an increase in the large-scale fraction of extreme precipitation and also strengthening circulation on extreme precipitation days. Compared to other CMIP5 models, the nonlinearity in CESM1 is among the largest. One implication is that the difference between CESM1 simulations with full forcing and with fixed aerosols cannot be used to isolate the response of extreme precipitation to aerosols, as the resulting climates are not equally warm.

Plain Language Summary Extreme precipitation can drive natural disasters like floods and landslides, so understanding and quantifying how it responds to warming is important. Climate models disagree on how much extreme precipitation changes in response to global warming in the tropics. Here we focus on trying to understand the response in just one climate model, CESM1. Some previous studies using this model assumed that the response of extreme precipitation for a given amount of warming is fixed. This is what we would expect if the change in extreme precipitation followed the amount of moisture in the atmosphere. However, we find that the response of extreme precipitation in the tropics to a given amount of warming is not fixed, and instead increases as the temperature warms. Changes in circulation and in the way the model produces precipitation accompany this behavior. Among other climate models, this behavior is shared by some but not all models. CESM1 has a larger increase in extreme precipitation change in response to warming than most models, and some lack this behavior entirely. The next generation of models that descend from CESM1 also do not share this behavior.

1. Introduction

Climate variability and change can often be approximated as linear: For example, the global average precipitation change from 0 to 1 °C of global warming is approximately the same as the change from 1 to 2° in climate model projections. However, for extreme precipitation, the response to warming in some models might increase as the warming itself increases—a nonlinear response. This type of response occurs in models with a tropical extreme precipitation response that deviates from the response of the rest of the intensity distribution, which has been called an "extreme mode" (Pendergrass & Hartmann, 2014). The extreme mode is one factor that contributes to the substantial variation in the magnitude of the tropical extreme precipitation response across climate models (O'Gorman, 2012). This variation in extreme precipitation response also influences nonextreme precipitation; models with larger increases in extreme precipitation have smaller increases or even decreases in nonextreme precipitation (Thackeray et al., 2018).

One framework for thinking about extreme precipitation change is that the precipitation rate in an extreme event is proportional to the product of moisture and circulation (measured by vertical velocity through the cloud base or by convergence of dry air in the boundary layer; Pendergrass & Gerber, 2016). In this framework, if moisture were to change at constant relative humidity with no change in circulation, then the extreme precipitation change would follow moisture, deviating only slightly from linearity ($\Delta r_x/r_x$, where r_x is extreme precipitation). In model projections, moisture changes at approximately constant relative humidity, but changes in circulation also contribute to extreme precipitation change (particularly its spatial pattern; Pfahl et al., 2017).

Despite indications that the response of extreme precipitation to warming may not be linear in all climate models, additivity is sometimes assumed. One approach that has been used to isolate the climate response to individual forcing agents is to take the difference between simulations in which many forcings vary over time and simulations in which one forcing is held fixed; this works when the response to each forcing is linear and thus additive. Two recent studies use this approach to try and isolate the extreme precipitation response to anthropogenic aerosol forcing (Lin et al., 2016; Zhao et al., 2018). However, the linearity of the extreme precipitation response to climate change in these simulations has not been established.

Here we investigate the response of extreme precipitation to climate change by focusing on one climate model, CESM1. We will show that the response of extreme precipitation in the tropics is actually nonlinear. Then we will show how this nonlinearity relates to parameterizations of precipitation, as well as changes in circulation and moisture. Next we will compare the response of extreme precipitation in CESM1 with other models from the CMIP5 cohort. Finally, we will consider the implications for isolating the response of extreme precipitation to GHG and anthropogenic aerosol forcings.

2. Methods

One challenge for studying extreme events is that they are rare; more samples improve our certainty in quantifying these events and how they change. Large ensembles of simulations enable greater sampling, widening the breadth of analyses that can be employed. We use two large ensembles of CESM1 simulations: the 40-member CESM1 Large Ensemble (CESM1-LE) (Kay et al., 2015) and a 20-member ensemble with fixed anthropogenic aerosols (hereafter CESM1-AA). The CESM1-LE is a set of fully coupled simulations at nominal 1° resolution, forced with historical estimates of natural and anthropogenic radiative forcings from 1920 to 2005 and the Representative Concentration Pathway (RCP) 8.5 scenario (Meinshausen et al., 2011) from 2006 to 2100. RCP8.5 is a high-emission scenario with large increases in GHGs over the 21st century and anthropogenic aerosol forcing, which increases until about 2030 and then subsequently decreases to low levels by the end of the century. Members are initialized from year 1920 of a historical simulation that begins in 1850; members are differentiated by adding small perturbations to atmospheric temperature [see Kay et al., 2015]. CESM1-AA is a 20-member set of simulations from 1920 to 2080, which are identical to the CESM1-LE except that energy-sector anthropogenic aerosols remain fixed at 1920 values. Like CESM1-LE, CESM1-AA members are initialized with small perturbations to atmospheric temperatures in 1920, using the same historical simulation as CESM1-LE. The variables we use here are monthly averaged reference height air temperature (TREFHT) and daily-averaged precipitation (convective and large-scale, PRECC and PRECL), zonal and meridional wind components at 850 hPa (U850 and V850), specific humidity in the lowest atmospheric layer (QBOT), and 500-hPa vertical velocity (OMEGA500, available for two members of the CESM1-LE).

We also compare CESM1 against the CMIP5 multimodel ensemble. We use fully coupled historical and RCP8.5 simulations from one ensemble member each of the 33 CMIP5 models with daily precipitation and monthly near-surface air temperature.

The response of extreme precipitation to global warming depends on how "extreme precipitation" is defined: The more extreme an event is, the larger its response is to warming (Pendergrass, 2018). Here we use the maximum daily accumulation of precipitation in each year (r_x, often called Rx1day; Zhang et al., 2011). r_x is extreme enough that its behavior does not merely follow mean precipitation (Pendergrass et al., 2015). At observing stations, r_x makes up 8.5% of total precipitation (Pendergrass & Knutti, 2018). r_x can be calculated for each year in each ensemble member, which facilitates analysis of changes over time. We calculate r_x at each grid point and then take area averages—for example, global, tropical, or extratropical.

3. Response of Extreme Precipitation to Warming in CESM1

In the CESM1-LE simulations, global-mean surface temperature increases little from 1920 to 1980 and subsequently climbs upward through 2100 (Figure 1a). Globally averaged r_x follows this overall pattern, with

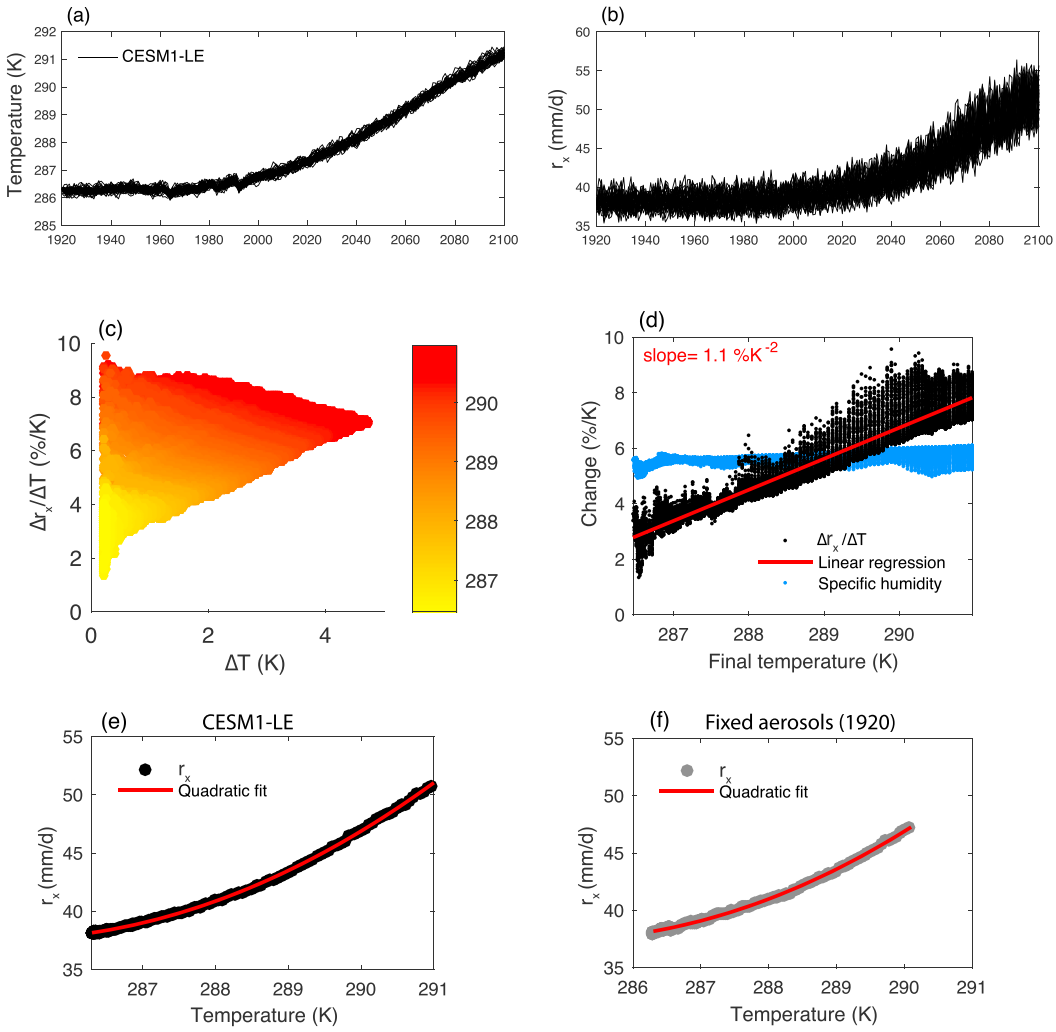

Figure 1. Nonlinear response of extreme precipitation to warming. Time series of (a) global-mean temperature and (b) maximum daily accumulation of precipitation each year (Rx1day or r_x) in the CESM1-LE 40-member ensemble. (c) $\Delta r_x/\Delta T$ between ensemble mean 10-year epoch pairs with >0.2-K global-mean temperature increase. Color indicates the global-mean temperature of the final epoch of the pair, T_{final}. (d) $\Delta r_x/\Delta T$ versus final epoch temperature (black). The best fit regression line is shown in red, with the slope indicated at the top left and the change in global, annual mean near surface specific humidity in blue. (e) Ensemble- and global-mean r_x versus temperature for each epoch from panel (d). The red line indicates the best fit quadratic polynomial. (f) As in Panel (e) for simulations with anthropogenic aerosols fixed at 1920 values (Figure S1).

little change until 1980 and a subsequent increase (Figure 1b). The variability of r_x across ensemble members is higher than for temperature, and it also increases over the 21st century.

To quantify the rate of change of r_x with warming, one approach is to calculate paired epoch differences. Some previous studies have, instead, regressed changes in extreme precipitation against changes in temperature (Lin et al., 2016; Pendergrass et al., 2015), but this assumes that the changes are linear. For our paired epoch differences, we choose 10-year epochs, averaging over all 40 ensemble members to reduce noise. We use all possible pairs of epochs, drawing both the initial and final epochs from the entire course of the simulation. After calculating global-mean temperature T and r_x for each epoch, we calculate the relative change normalized by warming ($\Delta r_x/\Delta T$, with units of % K^{-1}), which is the change in r_x divided by the average r_x during the base epoch and also ΔT. To avoid redundancy and division by zero, we exclude epoch pairs whose global-mean temperature change is less than +0.2 K in absolute value, which has the effect that each pair is a warmer epoch compared to a cooler epoch.

Examining $\Delta r_x/\Delta T$ as a function of ΔT, the relationship is not unique (Figure 1c). For small warming increments close to the lower threshold (+0.2 K), $\Delta r_x/\Delta T$ ranges from ~1% to ~9% K^{-1}. Moving toward larger ΔT, the range of $\Delta r_x/\Delta T$ converges to ~7% K^{-1} at around 5-K warming. In terms of when in the simulation each epoch pair occurs, the largest ΔT must involve initial epochs toward the beginning of the simulations (before ~1980) with those toward the end. The epoch pairs with smaller ΔT are from periods closer together in time, or from the beginning of the simulations. This raises the following question: If the rate of extreme precipitation change is not driven solely by temperature change, what other factors play a role?

Motivated by the observation that the variability of r_x increases with warming (Figure 1b), we examine $\Delta r_x/\Delta T$ as a function of the temperature of the final (warmer) epoch (T_{final}; Figures 1c and 1d). Unlike ΔT, there is a monotonic relationship between T_{final} and $\Delta r_x/\Delta T$—larger values of $\Delta r_x/\Delta T$ occur when the final epoch is warmer. Indeed, linear regression captures much of this relationship —the slope of the best fit regression line is 1.1% K^{-2}. There are also features that linear regression does not capture, including some systematic variation among ensemble members (e.g., ~287.5 K), which is related to large volcanic eruptions that cool all ensemble members simultaneously. All large volcanic eruptions in these simulations occur before 2000; none are present in the future emissions scenario from 2006 onward.

If $\Delta r_x/\Delta T$ is linearly related to T_{final}, then by simple calculus we should expect r_x to be quadratically related to T,

$$\frac{\mathrm{d}r_x}{dT} = aT,$$
$$\int \frac{dr_x}{dT} dT = \int (aT)\, dT,$$
$$rx = aT^2 + b.$$

Averaging each epoch globally and across all ensemble members, we see that this is indeed the case (Figure 1e). Furthermore, averaging across 40 ensemble members removes most noise, so the quadratic polynomial fit explains over 99.9% of the variance of the relationship between r_x and T.

Recall from section 1 that if circulation during extreme events did not change with warming, extreme precipitation intensity would change with roughly the rate of moisture increase. How does the change in extreme precipitation in these simulations compare to changes in moisture? In these simulations, global, annual average specific humidity in the bottom layer of the atmosphere increases by about 5% to 6% K^{-1} early in the simulation, rising slightly toward 6% K^{-1} by the end of the simulations, a rate slightly lower than Clausius-Clapeyron (Figure 1d). Specific humidity on the day of heaviest precipitation each year rises at a slightly smaller rate, between 4% and 5.5% K^{-1} (not shown). Clausius-Clapeyron is between 6% and 7% K^{-1} at these temperatures and decreases slightly with increasing temperature. The change in moisture contrasts starkly with $\Delta r_x/\Delta T$, which varies from ~3% K^{-1} at colder global-mean temperatures to ~8% K^{-1} at the warmest temperatures.

So far, we have examined the changes in globally averaged $\Delta r_x/\Delta T$. But previous work has shown that in models with large increases in extreme precipitation, these occur in the tropics, rather than the extratropics (O'Gorman, 2012; Pendergrass & Hartmann, 2014). Therefore, we next examine the spatial pattern of the nonlinearity in r_x. To do this, we calculate the slope of the regression line between $\Delta r_x/\Delta T$ at each gridpoint and global T_{final}: A larger slope indicates larger nonlinearity in r_x. For this calculation, we only use time periods from 2000 onward, to avoid the influence of volcanic eruptions.

The slope of $\Delta r_x/\Delta T$ versus T_{final} is positive across the deep tropical oceans and portions of the tropical continents (Figure 2a). Some regions of Africa have negative slopes. Most of the extratropics have smaller slopes. The spatial pattern has some similarities to the pattern of change in r_x (Figure 2b), such as the enhanced increases across much of the tropical oceans, but also some differences from it, for example, over southeast Asia. The spatial pattern of r_x change also bears some resemblance to mean precipitation change (Fischer et al., 2013; Pendergrass et al., 2017; Figure 2c): Both have increases in the tropical Pacific and Atlantic, the northern Indian Ocean, and some tropical land areas. But they differ in that mean precipitation also has regions of decrease.

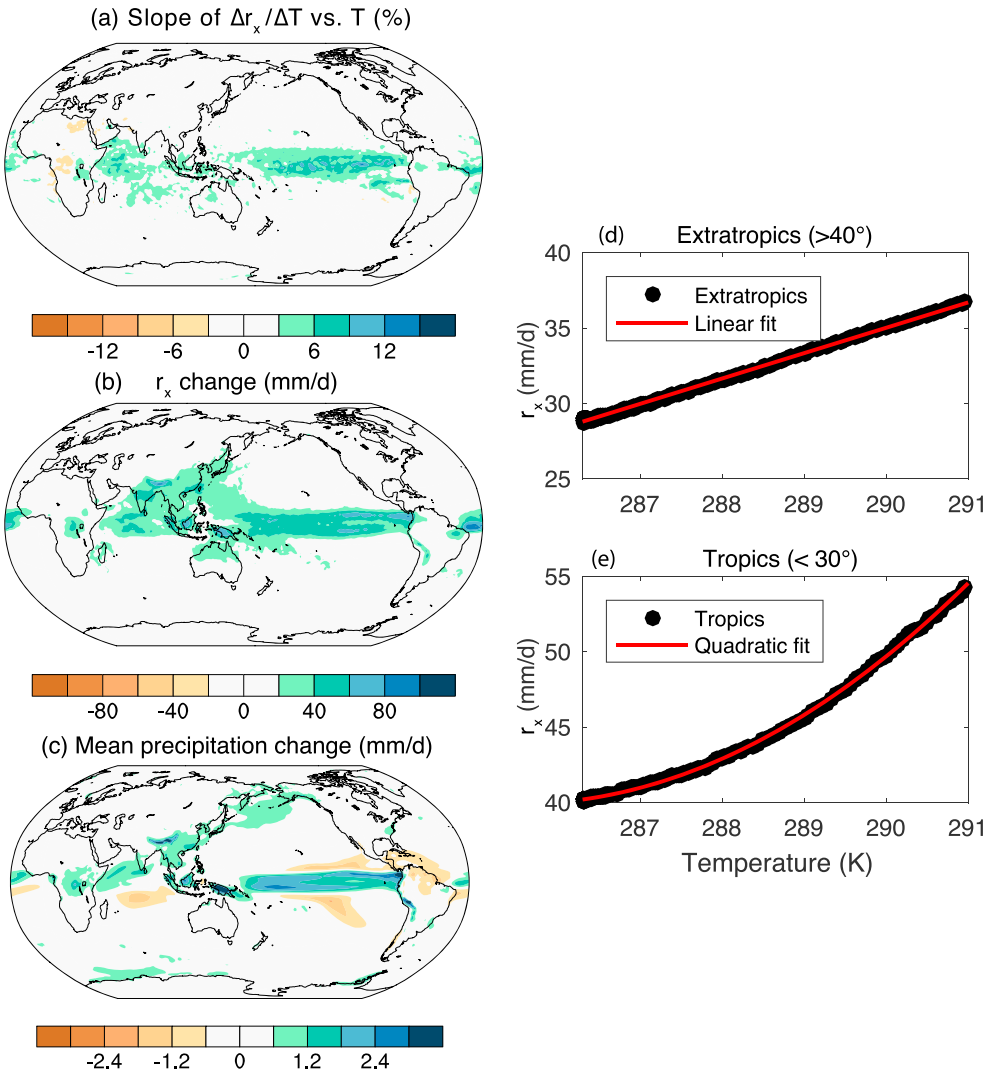

Figure 2. Geographical patterns of the nonlinear change in extreme precipitation. Maps of (a) slope of $\Delta r_x/\Delta T$ versus T_{final}, and for 2091–2100 minus 2000–2009, the (b) change in r_x and (c) mean precipitation change. r_x versus T (d) poleward of 40° latitude with linear fit and (e) equatorward of 30° with quadratic fit.

The spatial pattern motivates us to compare regional averages over the tropics, which we define as equatorward of 30° latitude, and the extratropics, poleward of 40°. The relationship between tropical r_x and T is captured well by a quadratic fit, while the relationship between extratropical r_x and T is nearly linear, consistent with the spatial pattern of nonlinearity. (Substituting local temperature change or temperature change on each r_x day for global-mean temperature produces a qualitatively similar result). The nonlinearity, then, arises from the tropics. It is dominated by the tropical oceans but remains present when the analysis is restricted to tropical land (Table S1 in the supporting information).

What drives the nonlinear relationship between tropical r_x and T? It has been argued that aerosol forcing drives a larger extreme precipitation increase than greenhouse gas forcing (Lin et al., 2016). To test whether the nonlinear extreme precipitation response is driven by aerosol forcing, we repeat the analysis using the CESM1-AA ensemble, with fixed aerosol forcing. The nonlinear behavior persists in these simulations (Figures 1f and S1), which indicates that it is not driven by these aerosols.

Precipitation in today's climate models, including CESM1 and all other CMIP5 models, is parameterized—via either convective (unresolved) or large-scale (resolved) parameterizations; so parameterizations are a potential driver of the nonlinearity. The fraction of r_x falling as resolved precipitation has a strong

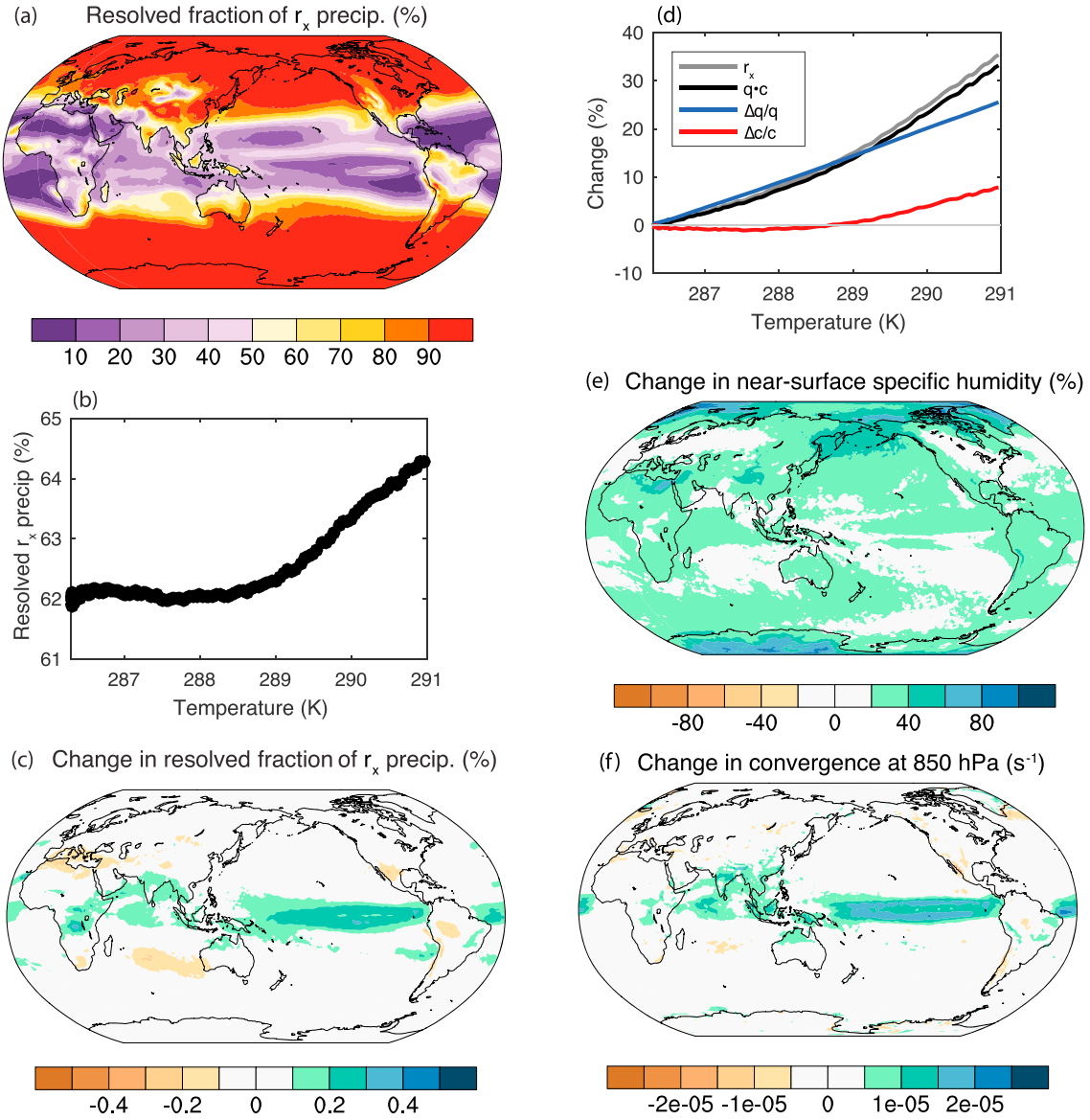

Figure 3. Parameterization of extreme precipitation; moisture and circulation components of change. (a) Fraction of r_x arising from resolved (large-scale) precipitation in CESM1, (b) global-mean fraction of resolved r_x at different global-mean temperatures, and (c) spatial pattern of the change in resolved fraction of r_x. (d) Scaling of r_x into circulation, c, and moisture, q, components: the change in r_x (gray), the change in the product of q and c (approximating r_x, black), the change in q alone (blue), and the change in c alone (red). Spatial pattern of the change in (e) near-surface specific humidity and (f) 850-hPa convergence on the day of r_x. See the supporting information for details.

dependence on latitude in CESM1—most extreme precipitation is resolved in the extratropics, while most is unresolved in the tropics (Figure 3a). In the tropics, there are also differences between precipitation over land and ocean; over land, more precipitation is resolved than over ocean. In response to warming, the fraction of r_x precipitation that is resolved increases from about 62% to just over 64%, particularly beyond 289 K (Figure 3b). The spatial pattern of the increase in resolved r_x fraction (Figure 3c) bears resemblance to the change in r_x itself, to the spatial pattern of the nonlinearity (Figure 2a), and also to the changes in mean precipitation (Figure 2c). The increase in resolved fraction of r_x probably plays a role in the nonlinearity, though some of this role could be merely that regions which newly find themselves in mean ascent (due to, e.g., the shifting Inter-Tropical Convergence Zone) have more resolved extreme precipitation.

The roles of circulation and moisture change can be decomposed using various scaling relationships (e.g., Norris et al., 2019; O'Gorman & Schneider, 2009). To estimate circulation throughout the CESM1-LE

simulations (given available model output), we use a single-level scaling between near-surface specific humidity and convergence at 850 hPa (Figure 3d). This scaling closely captures the changes in r_x, underestimating it slightly (the actual change is 35% compared to scaling of 33% at the end of the simulations). Moisture climbs steadily upward, nearly linearly, consistent with constant-relative humidity warming on r_x days. But convergence strength changes little until about 289-K global-mean temperature and subsequently increases, similar to the resolved fraction of r_x. Convergence at 850 hPa follows a similar trajectory to 500-hPa vertical velocity (Figure S3). The spatial pattern of moisture change (Figure 3e) resembles that expected based on constant-relative-humidity warming, dominated by polar amplification. But the spatial pattern of change in convergence shares many commonalities with the change in resolved fraction of r_x (Figure 3f).

Together these analyses show that the nonlinear increase in r_x in the tropics is associated with increasing circulation strength and also coincides with an increasing importance of resolved precipitation for r_x. Moisture changes and aerosol forcing, on the other hand, are not sources of nonlinearity.

4. Comparison With Other Climate Models

How does the nonlinear increase in r_x in CESM1 compare to that in other climate models? In the CMIP5 archive, most models have just one or a few simulations available. We therefore adapt the analysis to use one simulation from each model and compute the spatially averaged r_x and temperature over sliding 30-year windows. We start this analysis in 2000, after the effects of large volcanoes have faded. We calculate global $\Delta r_x/\Delta T$ for each epoch pair against T_{final} (following Figure 1d). We calculate the regression slope across all epoch pairs and sort the models from largest to smallest slope (Figure 4).

The relationships are noisier with just one ensemble member than with 40, despite averaging over 30- instead of 10-year periods (as in Figure 1c). If the extreme precipitation change were linear with respect to warming, $\Delta r_x/\Delta T$ would be constant, and so the slope of $\Delta r_x/\Delta T$ versus T_{final} would be zero. To test whether the regression slopes are nonzero, we assume slopes follow a normal distribution with standard deviation estimated from the CESM1-LE regression slopes and mean equal to the slope of each CMIP5 simulation and test whether this distribution includes zero at the 95% confidence level. Across CMIP5, 15 of the models have nonzero slopes, all of which are positive.

Among the models with the largest increases in $\Delta r_x/\Delta T$ with warming are those in the CESM family: CESM1-BGC, CESM1-CAM5, CCSM4, and NorESM1-M. While these models share heritage, they have similarities and differences. CESM1-BGC and CESM1-CAM5 have very few differences in configuration from the CESM1-LE; the differences in extreme precipitation response among these simulations are likely due only to internal variability. On the other hand, CCSM4 and CESM1-BGC have a different atmospheric physics package (CAM4), which includes differences in shallow convection, cloud microphysics and macrophysics, the aerosol model, and the radiation scheme. NorESM1-M descends from CCSM4, with an updated aerosol-cloud-radiation scheme (Bentsen et al., 2012).

Other models with large increases in $\Delta r_x/\Delta T$ with warming are GFDL-ESM-2M and IPSL-CM5A-LR. The GFDL-ESM family has the largest overall magnitude of extreme precipitation change among models, reaching 13–14% K^{-1} according to this particular measure. Previous work shows commensurately larger increases for more infrequent definitions of extreme precipitation (e.g., Pendergrass & Hartmann, 2014). This indicates that nonlinearities could account for some of the large increases of extreme precipitation in response to warming.

Repeating the analysis for the extratropical extreme precipitation (poleward of 40°), only 8 of the 33 models have a nonzero change in $\Delta r_x/\Delta T$ with T_{final}, which is positive in all cases; also, the magnitudes of change vary less among models. For the tropics, 14 models have a nonzero change in $\Delta r_x/\Delta T$ with T_{final}, also all positive. This is consistent with the nonlinearity arising from the tropics and with previous work showing that model uncertainty in extreme precipitation change arises from the tropics (O'Gorman, 2012).

Since temperature is related to $\Delta r_x/\Delta T$ in individual models, does it explain the variation across models? Indeed, T in 2000–2009 is not significantly correlated with $\Delta r_x/\Delta T$ or r_x across models; perhaps tuning precludes a relationship.

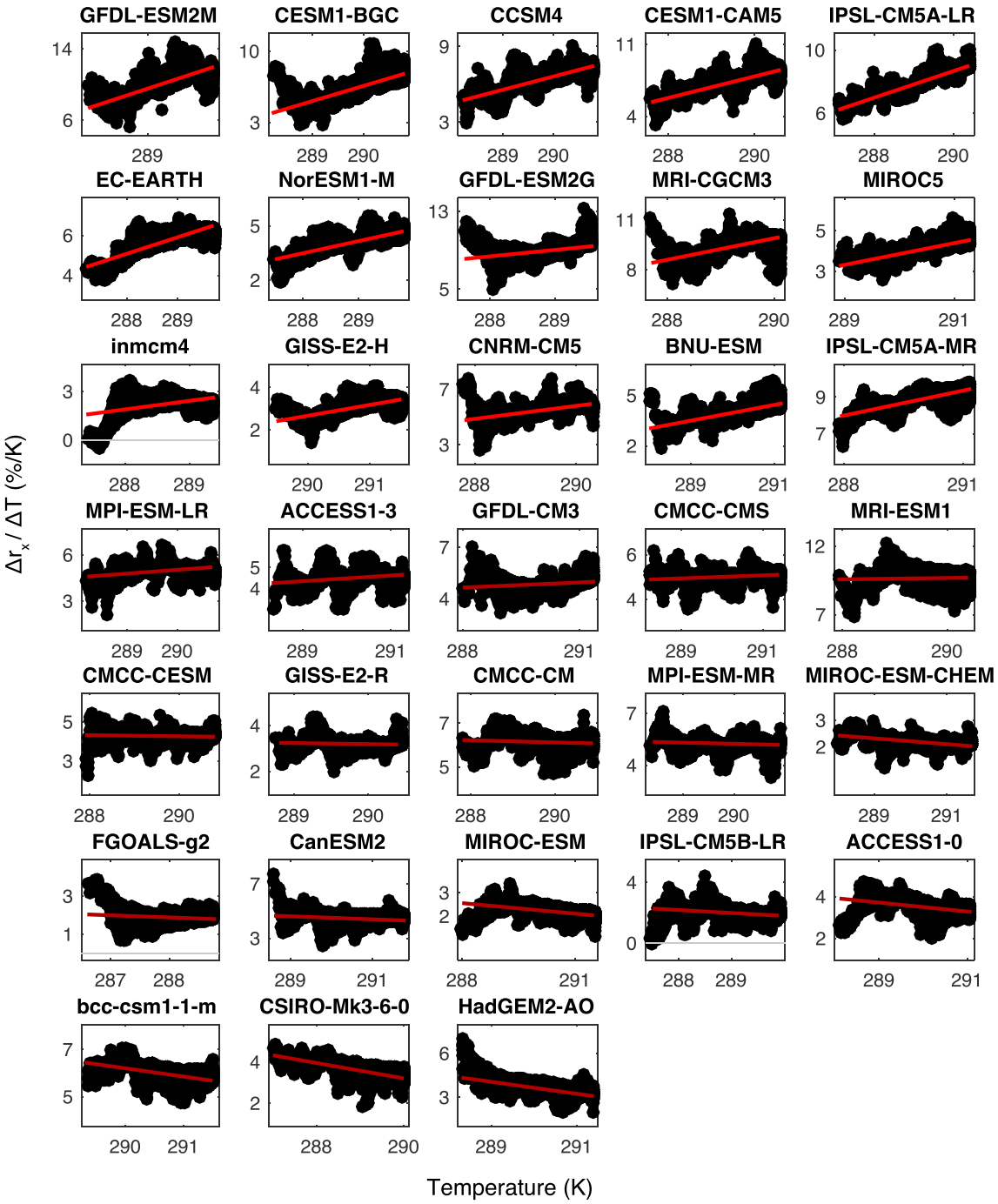

Figure 4. Nonlinearity across CMIP5 models. Global $\Delta r_x/\Delta T$ between epoch pairs versus global-mean T_{final} for each model. Best fit regression line for each simulation in red; bright red indicates that the slope is significantly different from zero, and dark red indicates it is not. The significance test assumes that slopes are normally distributed with mean equal to the simulation's slope and standard deviation equal to the maximum-likelihood-estimated standard deviation of slopes from CESM1-LE. Simulations are sorted from largest to smallest regression slope.

The CESM1 model has a variety of descendants in CMIP6, including CESM2 and E3SM. Applying the analysis to one transient carbon dioxide increase simulation with each of these models (Figure S2), both have increases in $\Delta r_x/\Delta T$ in response to warming, but the magnitudes are smaller than CESM1. In E3SM, the slope of $\Delta r_x/\Delta T$ versus T is 0.2% K^{-2}, and in CESM2, it is 0.4% K^{-2} (compared to 0.8–1.5% K^{-2} in for individual CESM1-LE members).

5. Implications for the Response of Extreme Precipitation to GHG and Aerosol Forcing

A nonlinear response of extreme precipitation to warming makes analysis techniques that implicitly or explicitly assume additivity problematic, for example, those of Lin et al. (2016) and Zhao et al. (2018). They approximated the response to aerosol forcing as the difference between the CESM1-LE and another 15-member CESM1 ensemble over 2005–2100 in which anthropogenic aerosols were held fixed at 2005 values, invoking an assumption of linearity. Using this approach, they found that $\Delta r_x/\Delta T$ is approximately two times larger for aerosol forcing than greenhouse gas forcing.

In RCP8.5, anthropogenic aerosol forcing increases from 2006 to 2030 and then subsequently decreases (see Pendergrass et al., 2015). The decrease of aerosols after 2030 drives additional global warming, beyond that from GHGs. As a result, the fixed-aerosol simulations have less global-mean warming than CESM1-LE (Figure S5). Given the nonlinear relationship between extreme precipitation and temperature documented here, we should expect the additional warming to drive an increase in extreme precipitation regardless of whether the warming is driven by aerosols or greenhouse gases—it occurs at the same rate in simulations with and without changes in anthropogenic aerosol forcing (Figure S1).

In contrast to extreme precipitation, global-mean precipitation is linear in CESM1 simulations (Figure S6). Lin et al. (2016) also find a large difference in the change in global-mean precipitation in response to GHGs and aerosols, which is expected from the differing effects of these forcings on atmospheric radiative fluxes, consistent with other studies. Some conclusions from Lin et al. are further affected by the use of moderate definitions of extreme precipitation, like R95p and R10—the precipitation falling in these events constitutes a large fraction of total precipitation and thus should be expected to behave more like mean precipitation than extreme precipitation (Pendergrass & Knutti, 2018).

6. Conclusions

Extreme precipitation—quantified here by the maximum amount of precipitation falling on a single day each year (r_x)—changes nonlinearly with respect to global-mean temperature in the tropics in CESM1. The nonlinearity is associated with strengthening circulation (the dynamic component) and with an increase in large-scale (resolved) precipitation with warming. The spatial patterns of the circulation change, the increase in large-scale extreme precipitation fraction, and the nonlinearity have many features in common. Mechanisms that we exclude as drivers of the nonlinear response are the change in moisture (the thermodynamic component) and anthropogenic aerosol forcing.

Among the CMIP5 cohort of models, the nonlinearity in CESM1 extreme precipitation is among the largest. CCSM4 also shares this large nonlinearity, but initial analysis with E3SM and CESM2 (which both descend from CESM1) indicate that they do not share this behavior.

A previous study mistook the nonlinearity in extreme precipitation in CESM1 for a response to aerosol forcing. Because the relationship between extreme precipitation and surface temperature is nonlinear, the responses of extreme precipitation to different forcing agents are not additive, and so the difference between simulations with many forcing agents and those that exclude one forcing does not accurately reflect the influence of that forcing agent on extreme precipitation.

One question arises from these findings: Is a nonlinear response of tropical extreme precipitation to warming realistic? Changes in circulation that increase as the climate state becomes warmer may be physical. The short observational record could present a challenge for documenting it on Earth. If the response of extreme precipitation were to grow with warming, then changes that have been observed so far would be smaller than what will occur moving into warmer climates in the future. Future work could seek relationships between observable present-day precipitation and nonlinear responses, for example, in terms of their spatial pattern. For the moment, this study shows that we cannot always assume that climate is linear—sometimes it is quadratic.

Acknowledgments
We thank Mark Webb, Jiawei Bao, and Steve Sherwood for helpful discussion. This material is based upon work supported by the National Center for Atmospheric Research, which is a major facility sponsored by the National Science Foundation (NSF) under Cooperative Agreement 1852977. Portions of this study were supported by the Regional and Global Model Analysis (RGMA) component of the Earth and Environmental System Modeling Program of the U.S. Department of Energy's Office of Biological and Environmental Research (BER) via NSF IA 1844590. CESM1-LE and CESM1-AA data are available from ESG at http://www.cesm.ucar.edu/projects/community-projects/LENS/data-sets.html (CESM1-AA is listed as "xaer"). CMIP5 model output is archived by PCMDI (available from https://pcmdi.llnl.gov/mips/cmip5). We also thank Urs Beyerle for CMIP5 data management. E3SM and CESM2 data are available online (from https://esgf-node.llnl.gov/search/e3sm/ and https://esgf-node.llnl.gov/search/cmip6/, respectively. The CESM project is supported primarily by the NSF.

References

Bentsen, M., Bethke, I., Debernard, J. B., Iversen, T., Kirkevåg, A., Seland, Ø., et al. (2012). The Norwegian Earth System Model, NorESM1-M – Part 1: Description and basic evaluation. *Geoscientific Model Development Discussion*, *5*(3), 2843–2931. https://doi.org/10.5194/gmdd-5-2843-2012

Fischer, E. M., Beyerle, U., & Knutti, R. (2013). Robust spatially aggregated projections of climate extremes. *Nature Climate Change*, *3*(12), 1033–1038. https://doi.org/10.1038/nclimate2051

Kay, J. E., Deser, C., Phillips, A., Mai, A., Hannay, C., Strand, G., et al. (2015). The community earth system model (CESM) large ensemble project: A community resource for studying climate change in the presence of internal climate variability. *Bulletin of the American Meteorological Society*, *96*(8), 1333–1349. https://doi.org/10.1175/BAMS-D-13-00255.1

Lin, L., Wang, Z., Xu, Y., & Fu, Q. (2016). Sensitivity of precipitation extremes to radiative forcing of greenhouse gases and aerosols. *Geophysical Research Letters*, *43*, 9860–9868. https://doi.org/10.1002/2016GL070869

Meinshausen, M., Smith, S. J., Calvin, K., Daniel, J. S., Kainuma, M. L. T., Lamarque, J. F., et al. (2011). The RCP greenhouse gas concentrations and their extensions from 1765 to 2300. *Climatic Change*, *109*, 213–241. https://doi.org/10.1007/s10584-011-0156-z

Norris, J., Chen, G., Neelin, J. D., Norris, J., Chen, G., & Neelin, J. D. (2019). Thermodynamic versus dynamic controls on extreme precipitation in a warming climate from the Community Earth System Model Large Ensemble. *Journal of Climate*, *32*, 1025–1045. https://doi.org/10.1175/JCLI-D-18-0302.1

O'Gorman, P. A. (2012). Sensitivity of tropical precipitation extremes to climate change. *Nature Geoscience*, *5*, 697–700. https://doi.org/10.1038/ngeo1568

O'Gorman, P. A., & Schneider, T. (2009). The physical basis for increases in precipitation extremes in simulations of 21st-century climate change. *Proceedings of the National Academy of Sciences of the United States of America*, *106*, 14,773–14,777. https://doi.org/10.1073/pnas.0907610106

Pendergrass, A. G. (2018). What precipitation is extreme? *Science*, 1072–1073. https://doi.org/10.1126/science.aat1871

Pendergrass, A. G., & Gerber, E. P. (2016). The rain is askew: Two idealized models relating vertical velocity and precipitation distributions in a warming world. *Journal of Climate*, *29*, 6445–6462. https://doi.org/10.1175/JCLI-D-16-0097.1

Pendergrass, A. G., & Hartmann, D. L. (2014). Changes in the distribution of rain frequency and intensity in response to global warming. *Journal of Climate*, *27*(22), 8372–8383. https://doi.org/10.1175/JCLI-D-14-00183.1

Pendergrass, A. G., & Knutti, R. (2018). The uneven nature of daily precipitation and its change. *Geophysical Research Letters*, *45*(21), 11,980–11,988. https://doi.org/10.1029/2018GL080298

Pendergrass, A. G., Knutti, R., Lehner, F., Deser, C., & Sanderson, B. M. (2017). Precipitation variability increases in a warmer climate. *Scientific Reports*, *7*(1), 17966. https://doi.org/10.1038/s41598-017-17966-y

Pendergrass, A. G., Lehner, F., Sanderson, B. M., & Xu, Y. (2015). Does extreme precipitation intensity depend on the emissions scenario? *Geophysical Research Letters*, *42*, 8767–8774. https://doi.org/10.1002/2015GL065854

Pfahl, S., O'Gorman, P. A., & Fischer, E. M. (2017). Understanding the regional pattern of projected future changes in extreme precipitation. *Nature Climate Change*, *7*(6), 423–427. https://doi.org/10.1038/nclimate3287

Thackeray, C. W., DeAngelis, A. M., Hall, A., Swain, D. L., & Qu, X. (2018). On the connection between global hydrologic sensitivity and regional wet extremes. *Geophysical Research Letters*, *45*(20). https://doi.org/10.1029/2018GL079698

Zhang, X., Alexander, L., Hegerl, G. C., Jones, P., Tank, A. K., Peterson, T. C., et al. (2011). Indices for monitoring changes in extremes based on daily temperature and precipitation data. *Wiley Interdisciplinary Reviews: Climate Change*, *2*(6), 851–870. https://doi.org/10.1002/wcc.147

Zhao, A. D., Stevenson, D. S., & Bollasina, M. A. (2018). The role of anthropogenic aerosols in future precipitation extremes over the Asian Monsoon Region. *Climate Dynamics*, *52*, 6257–6278. https://doi.org/10.1007/s00382-018-4514-7